Asian Journal of Chemistry; Vol. 37, No. 4 (2025), 882-892

ASIAN JOURNAL OF CHEMISTRY

https://doi.org/10.14233/ajchem.2025.33499

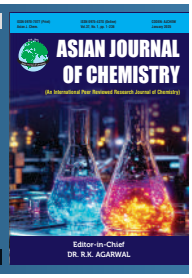

In silico Design, Synthesis and Biological Evaluation of Novel Chalcone Derivatives as Potent Tubulin-Targeting Anticancer Agents

KAILASH RANI[1], VIPIN KUMAR[2], RAKESH KUMAR SINDHU[3] and SOMDUTT MUJWAR[1,*]

[1]Department of Pharmaceutical Chemistry, Chitkara College of Pharmacy, Chitkara University, Rajpura-140401, India
[2]Broad Institute of MIT and Harvard. Cambridge, MA 02142, USA
[3]Department of Pharmacognosy and Phytochemistry, Sharda School of Pharmacy, Sharda University, Greater Noida-201310, India

*Corresponding author: E-mail: somduttmujwar@gmail.com

Received: 12 February 2025; *Accepted*: 12 March 2025; *Published online*: 29 March 2025; AJC-21950

Tubulin is an essential protein involved in microtubule dynamics that regulate mitotic cell division in normal cells. Specifically, the colchicine-binding site of tubulin serves as a therapeutic target to disrupt microtubule dynamics, inducing mitotic arrest and leading to cell death. In current study, we synthesized methoxy and fluorine substituted novel chalcones (**4a-o**) and the synthesized chalcone compounds showed promising anticancer activity by *in vitro* cell viability using the MTT assay in the lung cancer (A549) and breast cancer (MCF-7) cell lines and *in silico* docking simulations along with optimization of drug-like and pharmacokinetic properties. Among all compounds, (*E*)-1-(4,6-dimethoxybenzofuran-2-yl)-3-(4-methoxyphenyl)prop-2-en-1-one (**4f**) had the highest potency (IC_{50} = 23.9 ± 0.203 µM), followed by the fluorine substituted compound (*E*)-1-(4,6-dimethoxybenzofuran-2-yl)-3-(2,4,6-trifluorophenyl)prop-2-en-1-one (**4m**) (IC_{50} value of 35.44 µM). Moreover, compound **4f** demonstrated an excellent docking interaction (-9.94 kcal/mol) with the key residues Met-259, Leu-255 and Ala-250 at colchicine-binding pocket of tubulin against millepachine, which is similar to the millepachine binding site of tubulin, suggesting a mechanism of action that may potentially affect microtubule dynamics. Additionally, compound **4f** identified promising drug-like properties, physico-chemical and pharmacokinetic characteristics.

Keywords: Chalcone, Tubulin, Anticancer activity, Molecular docking, ADMET.

INTRODUCTION

Cancer involves uncontrolled mitotic cell division and metastasis caused by genetic defects and mutations that result in abnormal cell proliferation [1,2]. According to the International Agency for Research on Cancer (IARC), with an estimated 20 million new cases and 9.7 million deaths worldwide by 2022, lung cancer is the most prevalent and lethal form of cancer and implementing effective prevention strategies can significantly reduce the increasing global cancer burden [1,3]. Over the past few decades, the scientific community has successfully developed new technologies and drugs to treat cancer. Moreover, conventional therapies, such as chemotherapy and radiation, have shown efficacy; however, their non-selectivity and severe side effects emphasize the need for novel anticancer agents with enhanced potency and reduced toxicity [4-6].

Recent advances in molecular oncology have highlighted tubulin as a key structural protein essential for microtubule assembly, intracellular transport, cell shape maintenance, cell motility and mitotic spindle formation, critical targets for disrupting cancer progression [7-10]. Tubulin-targeting agents (*e.g.* paclitaxel, colchicine, vincristine and vinblastine) have been shown to have the ability to disrupt mitotic spindle assembly, resulting in mitotic arrest and apoptosis [6,8-12]. Moreover, colchicine site inhibitors remain an attractive target for their dual role in disrupting mitosis, functioning as vascular disrupting agents by blocking blood supply to solid tumors (Fig. 1, A-II, III) [13-16].

Chalcones are α,β-unsaturated ketones that can be easily synthesized by the condensation of aldehydes and ketones and undergo a one-step condensation reaction. Millepachine, a naturally occurring chalcone containing a 2,2-dimethylbenzopyran moiety, has shown *in vitro* anticancer activity [17,18]. Later, it was shown that millepachine binds to tubulin, as demonstrated by *in vitro* and docking studies (Fig. 1, A-I). In addition, chalcone, MDL 27048, also exhibited anticancer activity by

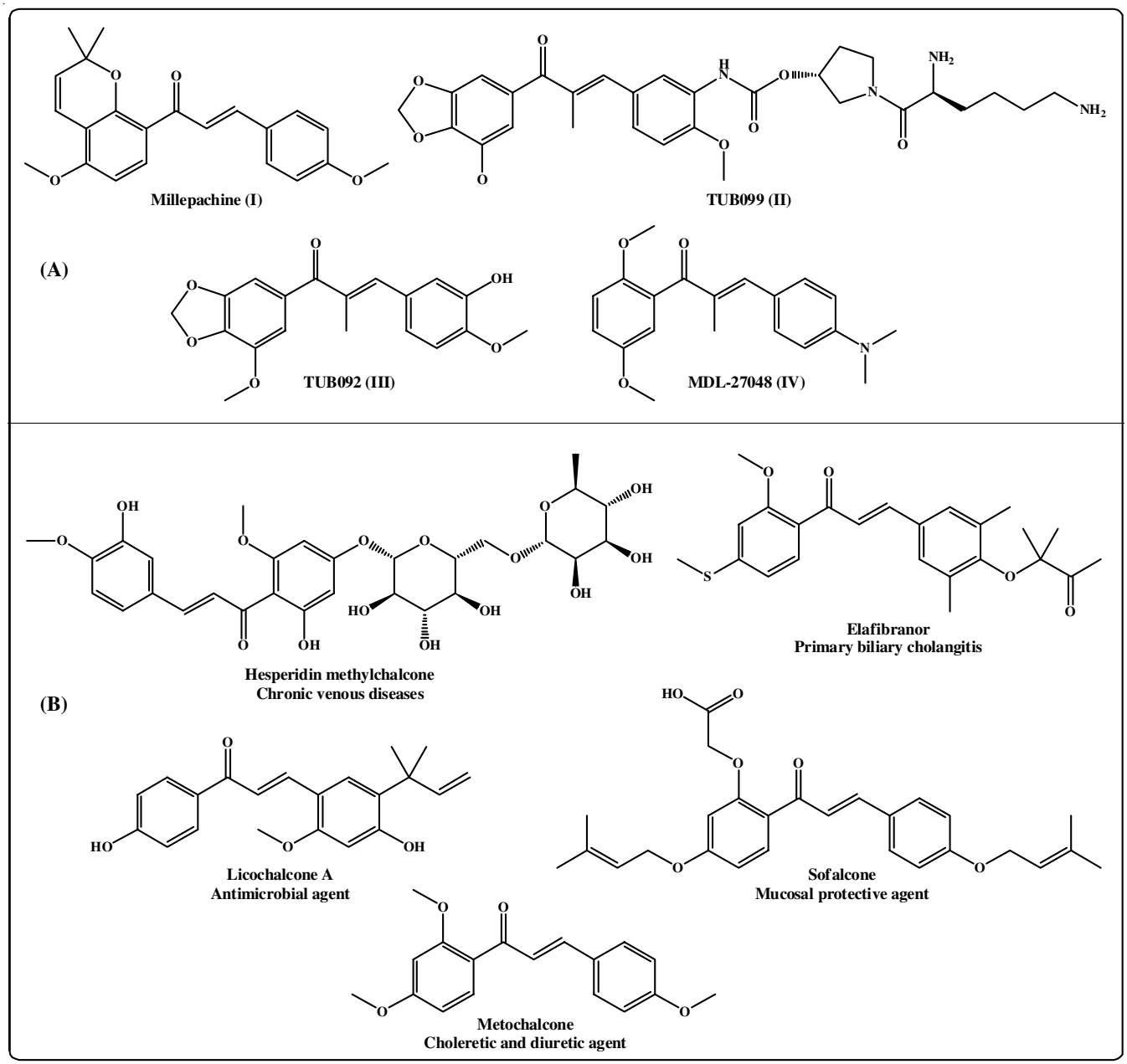

Fig. 1. Chemical structures of chalcones. The tubulin binding (A) and clinically approved (B)

interacting with tubulins [19] as illustrated in Fig. 1, A-IV. Moreover, chalcone-based drugs are used in clinical settings (Fig. 1B). Therefore, owing to the simplicity and ease of their synthesis, an attempt is made to design novel chalcone molecules.

This study aimed to design and evaluate new dimethoxy benzofuran-chalcones against the colchicine site of tubulin. Previous studies [20-26] on benzofuran and chalcone hybrids demonstrated enhanced binding and selectivity towards the colchicine site of tubulin, significantly improving their anticancer activity compared to other colchicine inhibitors. This is primarily due to the fused heterocyclic ring structure of benzofuran, which enhances hydrophobic interactions and hydrogen bonding, leading to increased binding affinity [23]. The specific arrangement of substituents on the chalcone scaffold (**Scheme-I**) allows for optimal fitting within the colchicine binding site, such as natural colchicine, causing microtubule destabilization, which is crucial for inducing mitotic arrest and apoptosis in cancer cells by activation of the caspase-3 pathway, further contributing to their anticancer efficacy [27-29]. The structure-activity relationship (SAR) based on *in vitro* cytotoxicity activity and docking interactions and *in silico* physico-chemical and pharmacokinetic properties to develop potent new anticancer agents.

EXPERIMENTAL

All chemical reagents and solvents were of synthetic grade. NMR spectra were recorded in $CDCl_3$ or dimethy sulfoxide-d_6 (DMSO-d_6) solvent. TLC was performed on a silica gel aluminum plate (Merck, Germany). Post-data analysis was performed using the UV-Win software. Human lung carcinoma

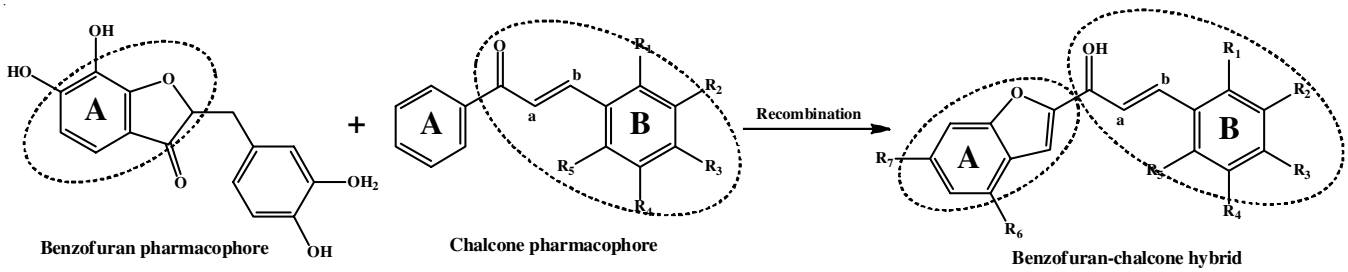

Scheme-I: Schematic representation of dimethoxy benzofuran-chalcone scaffold designing. Ring A (highlighted green) represents the benzofuran pharmacophore, while Ring B corresponds to the α,β-unsaturated ketone chalcone pharmacophore

(A549) and breast cancer (MCF-7) cell lines were purchased from NCCS (Pune, India). Biological data analysis was performed using GraphPad Prism 10.4 and Microsoft Excel software.

The synthesized compounds were analyzed using ^{1}H NMR and ^{13}C NMR spectroscopy. Additionally, mass spectrometry (ESI-MS) was used to determine the molecular weights of the synthesized compounds. Notably, ^{1}H NMR spectra revealed a coupling constant > J = 15.0 Hz for both a and b-hydrogens, indicating an *E*-configuration of the chalcone structures [30].

Synthesis of benzofuran-chalcone scaffold (3): The dimethoxy benzofuran ketone as starting material synthesized was adapted from the published procedure [31-34]. In brief, K_2CO_3 (1.82 g, 13.2 mmol) was added to 30 mL acetone in a 100 mL round bottom flask. The resulting suspension was stirred and 2.0 g (11.0 mmol) of 2-hydroxy-4,6-dimethoxybenzaldehyde was added, followed by addition of 1.1 mL (12.5 mmol) of chloroacetone. The mixture was refluxed for 6 h, filtered through a cotton plug, rinsed with acetone and the combined organic solution was evaporated. The remaining residues were subjected to flash chromatography using a 30% ethyl acetate/hexane mixture to obtain a white solid product with 70% yield.

General procedure for synthesis of benzofuran-chalcone derivatives (4a-o): The experimental protocol involved the addition of 500 mg (2.3 mmol) of 1-(4,6-dimethoxybenzofuran-2-yl)ethan-1-one to 20 mL methanol. The mixture was stirred for 20 min at 40 ºC to ensure the complete solubilization of ketone substrate. Subsequently, 1.1 equiv. of aldehyde was added and then the mixture was stirred for 5 min, followed by adding one equiv. of $Ba(OH)_2$ and the reaction mixture was continuously stirred until completion (~ 6 h). The organic solvent was evaporated and 20 mL water was added to the residue and finally the pH was adjusted to neutral using 1 M HCl. The coloured suspension was filtered and washed with water. The solid residue was stirred in 25 mL ethanol and the solid was filtered and washed with ethanol followed by diethyl ether (**Scheme-II**). Finally, the product was dried under high vacuum.

1-(4,6-Dimethoxybenzofuran-2-yl)ethan-1-one (3): Yield: 70%; m.f.: $C_{12}H_{12}O_4$; yellow colour; ^{1}H NMR (400 MHz, $CDCl_3$) δ ppm: 7.54 (s, 1H), 6.66 (s, 1H), 6.33 (d, J = 1.9 Hz, 1H), 3.93 (s, 3H), 3.88 (s, 3H), 2.55 (s, 3H); ^{13}C NMR (101 MHz, $CDCl_3$) δ ppm: 187.3, 162.6, 158.0, 155.2, 151.1, 112.1, 112.1, 95.2, 88.0, 55.9, 55.7, 26.0. ESI-MS (*m/z*): $[M + H]^+$ calculated at 221.08, found 221.22.

(*E*)-1-(4,6-Dimethoxybenzofuran-2-yl)-3-(4-fluorophenyl)prop-2-en-1-one (4a): Yield: 41%; m.f.: $C_{19}H_{15}FO_4$; light-yellow colour; ^{1}H NMR (400 MHz, $CDCl_3$) δ ppm: 7.88 (d, J = 15.8 Hz, 1H), 7.74-7.64 (m, 3H), 7.44 (d, J = 15.8 Hz, 1H), 7.14 (t, J = 8.6 Hz, 2H), 6.71 (s, 1H), 6.36 (d, J = 1.8 Hz, 1H), 3.95 (s, 3H), 3.90 (s, 3H); ^{13}C NMR (101 MHz, $CDCl_3$) δ ppm: 178.3 (C=O), 165.4, 162.9, 162.8, 158.2, 155.3, 142.3, 131.1, 131.1, 130.5, 130.4, 121.1, 121.1, 116.0, 112.4, 112.2, 95.3, 88.1, 55.9, 55.7. ^{19}F NMR (376 MHz, $CDCl_3$) δ ppm: -109.03; ESI-MS (*m/z*): $[M + H]^+$ calculated at 327.10, found 327.22.

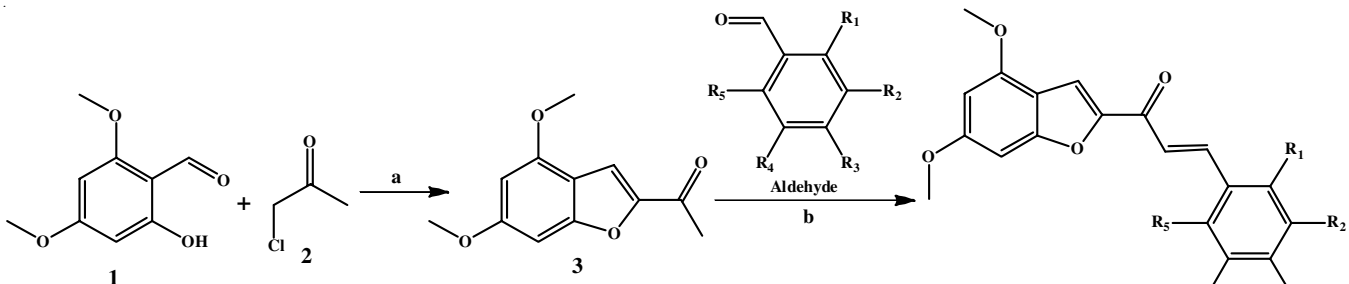

4a: $R_1 = R_2 = R_4 = R_5 = H$, $R_3 = F$
4b: $R_1 = R_2 = R_5 = H$, $R_3 = R_4 = F$
4c: $R_2 = R_3 = R_5 = H$, $R_1 = R_4 = F$
4d: $R_1 = R_2 = R_4 = R_5 = H$, $R_3 = CF_3$
4e: $R_2 = R_3 = R_4 = H$, $R_1 = R_5 = F$
4f: $R_1 = R_2 = R_4 = R_5 = H$, $R_3 = OCH_3$
4g: $R_3 = R_4 = R_5 = H$, $R_1 = R_2 = OCH_3$
4h: $R_1 = R_3 = R_5 = H$, $R_2 = R_4 = OCH_3$
4i: $R_3 = R_4 = R_5 = H$, $R_1 = R_5 = OCH_3$
4j: $R_2 = R_3 = R_4 = R_5 = H$, $R_1 = F$
4k: $R_2 = R_4 = R_5 = H$, $R_1 = R_3 = F$
4l: $R_4 = R_5 = H$, $R_1 = R_2 = R_3 = F$
4m: $R_2 = R_4 = H$, $R_1 = R_3 = R_5 = F$
4n: $R_1 = R_2 = R_3 = R_4 = R_5 = H$
4o: $R_1 = R_2 = H$, $R_3 = R_4 = R_5 = OCH_3$

Scheme-II: Synthesis of dimethoxy benzofuran-chalcone derivatives (**4a-o**). Regents and conditions: (a) K_2CO_3, acetone, reflux, 8 h; (b) MeOH, $Ba(OH)_2$, 6 h, 40 ºC

(*E*)-3-(3,4-Difluorophenyl)-1-(4,6-dimethoxybenzofuran-2-yl)prop-2-en-1-one (4b): Yield: 33%; m.f.: $C_{19}H_{14}F_2O_4$; yellow colour; ^{1}H NMR (400 MHz, $CDCl_3$) δ ppm: 7.81 (d, *J* = 15.6 Hz, 1H, H-3), 7.72 (s, 1H), 7.56-7.48 (m, 1H), 7.44-7.40 (m, 2H), 7.27-7.19 (m, 1H), 6.71 (s, 1H), 6.36 (d, *J* = 1.8 Hz, 1H), 3.95 (s, 3H), 3.90 (s, 3H); ^{13}C NMR (101 MHz, $CDCl_3$) δ ppm: 177.9, 162.9, 158.3, 155.4, 152.0, 141.2, 141.1, 141.1, 132.2, 132.1, 132.1, 132.1, 125.5, 125.5, 125.4, 125.4, 122.3, 122.2, 118.0, 117.8, 116.6, 116.4, 112.6, 112.4, 95.4, 88.0, 55.9, 55.7; ^{19}F NMR (376 MHz, $CDCl_3$) δ ppm: -133.66, -133.71, -136.51, -136.56. ESI-MS (*m/z*): $[M + H]^+$ calculated at 345.09, found 345.48.

(*E*)-3-(2,5-Difluorophenyl)-1-(4,6-dimethoxybenzofuran-2-yl)prop-2-en-1-one (4c): Yield: 89%; m.f.: $C_{19}H_{14}F_2O_4$; orange colour; ^{1}H NMR (400 MHz, $CDCl_3$) δ 7.95 (d, *J* = 16.0 Hz, 1H, H-3), 7.73 (s, 1H), 7.57 (d, *J* = 15.9 Hz, 1H), 7.40-7.36 (m, 1H), 7.16-7.08 (m, 2H), 6.72 (s, 1H), 6.36 (d, *J* = 1.8 Hz, 1H), 3.95 (s, 3H), 3.90 (s, 3H); ^{13}C NMR (101 MHz, $CDCl_3$) δ ppm: 177.9, 163.0, 158.4, 155.4, 152.0, 135.0, 135.0, 134.9, 124.8, 124.8, 124.3, 124.2, 124.2, 124.1, 118.4, 118.4, 118.2, 118.1, 117.6, 117.6, 117.4, 117.3, 115.3, 115.3, 115.1, 115.1, 112.8, 112.4, 95.4, 88.0, 55.9, 55.7. ^{19}F NMR (376 MHz, $CDCl_3$) δ ppm: -118.25, -118.30, -119.26, -119.31. ESI-MS (*m/z*): $[M + H]^+$ calculated at 345.09, found 345.48.

(*E*)-1-(4,6-Dimethoxybenzofuran-2-yl)-3-(4-(trifluoromethyl)phenyl)prop-2-en-1-one (4d): Yield: 49%; m.f.: $C_{20}H_{15}F_3O_4$; dark-yellow colour; ^{1}H NMR (400 MHz, $CDCl_3$) δ ppm: 7.90 (d, *J* = 15.8 Hz, 1H), 7.77 (d, *J* = 8.4 Hz, 2H), 7.73 (s, 1H), 7.69 (d, *J* = 8.4 Hz, 2H), 7.56 (d, *J* = 15.6 Hz, 1H), 6.70 (s, 1H), 6.35 (d, *J* = 1.8 Hz, 1H), 3.95 (s, 3H), 3.90 (s, 3H); ^{13}C NMR (101 MHz, $CDCl_3$) δ ppm: 177.9, 163.0, 158.4, 155.4, 152.0, 141.5, 138.2, 132.4, 132.0, 131.7, 131.4, 128.6, 126.0, 125.9, 125.9, 125.8, 123.6, 112.8, 112.4, 95.4, 88.0, 55.9, 55.7. ^{19}F NMR (376 MHz, $CDCl_3$) δ ppm: -62.84. ESI-MS (*m/z*): $[M + H]^+$ calculated at 377.10, found 377.24.

(*E*)-3-(2,6-Difluorophenyl)-1-(4,6-dimethoxybenzofuran-2-yl)prop-2-en-1-one (4e): Yield: 80%, m.f.: $C_{19}H_{14}F_2O_4$; pale-yellow colour; ^{1}H NMR (400 MHz, $CDCl_3$) δ ppm: 8.00 (d, *J* = 16.1 Hz, 1H), 7.78 (d, *J* = 16.1 Hz, 1H), 7.71 (s, 1H), 7.41-7.31 (m, 1H), 7.00 (t, *J* = 8.6 Hz, 2H), 6.72 (s, 1H), 6.35 (d, *J* = 1.8 Hz, 1H), 3.95 (s, 3H), 3.90 (s, 3H); ^{13}C NMR (101 MHz, $CDCl_3$) δ ppm: 178.3, 163.4, 163.3, 162.9, 160.8, 160.8, 158.4, 155.3, 152.1, 131.4, 131.2, 131.1, 129.5, 129.4, 129.4, 127.0, 126.9, 126.8, 113.1, 113.0, 112.8, 112.4, 112.3, 112.1, 112.0, 112.0, 111.9, 111.8, 111.8, 95.4, 88.1, 55.9, 55.7; ^{19}F NMR (376 MHz, $CDCl_3$) δ ppm: -109.47. ESI-MS (*m/z*): $[M + H]^+$ calculated at 345.09, found 344.94.

(*Z*)-1-(4,6-Dimethoxybenzofuran-2-yl)-3-(4-methoxyphenyl)prop-2-en-1-one (4f): Yield: 70%, m.f.: $C_{20}H_{18}O_5$; yellow colour; ^{1}H NMR (400 MHz, $CDCl_3$) δ ppm: 7.89 (d, *J* = 15.6 Hz, 1H), 7.68 (s, 1H), 7.64 (d, *J* = 8.8 Hz, 2H), 7.39 (d, *J* = 15.6 Hz, 1H), 6.96 (d, *J* = 8.8 Hz, 2H), 6.71 (s, 1H), 6.34 (d, *J* = 1.8 Hz, 1H), 3.94 (s, 3H), 3.89 (s, 3H), 3.88 (s, 3H); ^{13}C NMR (101 MHz, $CDCl_3$) δ ppm: 178.6, 162.6, 161.7, 158.1, 155.2, 152.4, 143.5, 130.3, 127.6, 119.0, 114.4, 112.4, 111.7, 95.2, 88.1, 55.9, 55.7, 55.4. ESI-MS (*m/z*): $[M + H]^+$ calculated at 339.12, found 339.52.

(*E*)-1-(4,6-Dimethoxybenzofuran-2-yl)-3-(2,3-dimethoxyphenyl)prop-2-en-1-one (4g): Yield: 73%, m.f.: $C_{21}H_{20}O_6$; yellow colour; ^{1}H NMR (400 MHz, $CDCl_3$) δ ppm: 8.21 (d, *J* = 15.9 Hz, 1H), 7.69 (s, 1H), 7.58 (d, *J* = 15.9 Hz, 1H), 7.33 (d, *J* = 7.9 Hz, 1H), 7.12 (t, *J* = 8.0 Hz, 1H), 6.99 (d, *J* = 8.2 Hz, 1H), 6.72 (s, 1H), 6.35 (s, 1H), 3.95 (s, 3H), 3.93 (s, 3H), 3.92 (s, 3H), 3.90 (s, 3H); ^{13}C NMR (101 MHz, $CDCl_3$) δ ppm: 178.7, 162.7, 158.2, 155.3, 153.3, 152.4, 149.1, 138.5, 129.1, 124.2, 122.9, 119.7, 114.2, 112.4, 112.1, 95.3, 88.1, 61.4, 55.9, 55.9, 55.7. ESI-MS (*m/z*): $[M + H]^+$ calculated at 369.13, found 369.0.

(*E*)-1-(4,6-Dimethoxybenzofuran-2-yl)-3-(3,5-dimethoxyphenyl)prop-2-en-1-one (4h): Yield: 86%, m.f.: $C_{21}H_{20}O_6$; light-yellow colour; ^{1}H NMR (400 MHz, $CDCl_3$) δ ppm: 7.84 (d, *J* = 15.7 Hz, 1H), 7.71 (s, 1H), 7.46 (d, *J* = 15.7 Hz, 1H), 6.83 (d, *J* = 2.3 Hz, 2H), 6.72 (s, 1H), 6.56 (t, *J* = 2.3 Hz, 1H), 6.36 (d, *J* = 1.8 Hz, 1H), 3.96 (s, 3H), 3.90 (s, 3H), 3.88 (s, 6H); ^{13}C NMR (101 MHz, $CDCl_3$) δ ppm: 178.4, 162.8, 161.1, 158.3, 155.3, 152.2, 143.7, 136.7, 121.8, 12.4, 112.3, 106.4, 102.9, 95.3, 88.1, 55.9, 55.7, 55.5. ESI-MS (*m/z*): $[M + H]^+$ calculated at 369.13, found 369.26.

(*E*)-1-(4,6-Dimethoxybenzofuran-2-yl)-3-(2,6-dimethoxyphenyl)prop-2-en-1-one (4i): Yield: 93%; m.f.: $C_{21}H_{20}O_6$; yellow colour; ^{1}H NMR (400 MHz, $CDCl_3$) δ ppm: 8.38 (d, *J* = 15.9 Hz, 1H, , H-3), 7.93 (d, *J* = 16.0 Hz, 1H), 7.63 (s, 1H), 7.31 (t, *J* = 8.4 Hz, 1H), 6.72 (s, 1H), 6.60 (d, *J* = 8.3 Hz, 2H), 6.35 (s, 1H), 3.96-3.95 (m, 9H), 3.89 (s, 3H); ^{13}C NMR (101 MHz, $CDCl_3$) δ ppm: 180.1, 162.3, 160.5, 158.1, 155.1, 152.9, 134.7, 131.6, 124.1, 12.9, 12.9, 12.9, 112.4, 111.6, 103.8, 95.1, 88.2, 55.9, 55.9, 55.7. ESI-MS (*m/z*): $[M + H]^+$ Calculated for 369.13, found 369.01.

(*E*)-1-(4,6-Dimethoxybenzofuran-2-yl)-3-(2-fluorophenyl)prop-2-en-1-one (4j): Yield: 79%; m.f.: $C_{19}H_{15}FO_4$; light yellow colour; ^{1}H NMR (400 MHz, $CDCl_3$) δ ppm: 8.01 (d, *J* = 16.0 Hz, 1H), 7.74-7.66 (m, 2H), 7.61 (d, *J* = 15.9 Hz, 1H), 7.45-7.37 (m, 1H), 7.26-7.12 (m, 2H), 6.71 (s, 1H), 6.35 (d, *J* = 1.8 Hz, 1H), 3.95 (s, 3H), 3.90 (s, 3H); ^{13}C NMR (101 MHz, $CDCl_3$) δ ppm: 178.4, 163.1, 162.8, 160.6, 158.3, 155.3, 152.2, 136.4, 131.9, 131.8, 130.0, 130.0, 124.5, 124.5, 124.0, 123.9, 123.0, 122.9, 116.5, 16.2, 112.5, 112.4, 95.3, 88.1, 55.9, 55.7; ^{19}F NMR (376 MHz, $CDCl_3$) δ ppm: -112.99. ESI-MS (*m/z*): $[M + H]^+$ calculated at 327.10, found 326.92.

(*E*)-3-(2,4-Fluorophenyl)-1-(4,6-dimethoxybenzofuran-2-yl)prop-2-en-1-one (4k): Yield: 96%; m.f.: $C_{19}H_{14}F_2O_4$; light yellow colour; ^{1}H NMR (400 MHz, $CDCl_3$) δ ppm: 7.94 (d, *J* = 15.9 Hz, 1H), 7.75-7.64 (m, 2H), 7.55 (d, *J* = 15.9 Hz, 1H), 7.02-6.88 (m, 2H), 6.71 (s, 1H), 6.35 (d, *J* = 2.0 Hz, 1H), 3.95 (s, 3H), 3.90 (s, 3H); ^{13}C NMR (101 MHz, $CDCl_3$) δ ppm: 178.2, 162.9, 158.3, 155.3, 152.1, 135.4, 131.2, 131.1, 131.1, 131.0, 123.5, 123.5, 123.5, 123.4, 119.6, 119.5, 119.5, 119.4, 112.6, 112.4, 112.3, 112.2, 112.1, 112.0, 105.1, 104.8, 104.6, 95.4, 88.1, 55.9, 55.7; ^{19}F NMR (376 MHz, $CDCl_3$) δ ppm: -105.58, -105.60, -108.46, -108.49. ESI-MS (*m/z*): $[M + H]^+$ calculated at 345.09, found 345.23.

(*E*)-1-(4,6-Dimethoxybenzofuran-2-yl)-3-(2,3,4-trifluorophenyl)prop-2-en-1-one (4l): Yield: 83%; m.f.: $C_{19}H_{13}F_3O_4$; light-yellow colour; yield 83%; ^{1}H NMR (400 MHz, $CDCl_3$)

δ ppm: 7.88 (d, *J* = 16.0 Hz, 1H), 7.71 (s, 1H), 7.58 (d, *J* = 15.9 Hz, 1H), 7.45-7.36 (m, 1H), 7.10-7.01 (m, 1H), 6.71 (s, 1H), 6.35 (d, *J* = 1.8 Hz, 1H), 3.95 (s, 3H), 3.90 (s, 3H); ^{13}C NMR (101 MHz, $CDCl_3$) δ ppm: 177.8, 163.0, 158.4, 155.4, 151.9, 134.5, 124.7, 124.6, 124.6, 124.6, 124.6, 124.6, 123.8, 123.8, 123.7, 123.7, 120.9, 120.9, 120.8, 120.8, 112.9, 112.8, 112.7, 112.6, 112.6, 112.4, 95.4, 88.0, 55.9, 55.7; ^{19}F NMR (376 MHz, $CDCl_3$) δ ppm: -130.19, -130.22, -130.24, -130.27, -134.05, -134.08, -134.11, -134.13, -159.34, -159.39, -159.45. ESI-MS (*m/z*): $[M + H]^+$ calculated at 363.08, found 363.21.

(*E*)-1-(4,6-Dimethoxybenzofuran-2-yl)-3-(2,4,6-trifluorophenyl)prop-2-en-1-one (4m): Yield: 87%; m.f.: $C_{19}H_{13}F_3O_4$; yellow colour; ^{1}H NMR (400 MHz, $CDCl_3$) δ ppm: 7.89 (d, *J* = 16.1 Hz, 1H), 7.73-7.66 (m, 2H), 6.76 (t, *J* = 8.7 Hz, 2H), 6.71-6.66 (m, 1H), 6.33 (d, *J* = 1.8 Hz, 1H), 3.93 (s, 3H), 3.88 (s, 3H). ^{13}C NMR (101 MHz, $CDCl_3$) δ ppm: 178.3, 163.9, 163.8, 163.8, 163.7, 163.1, 161.4, 161.3, 161.2, 161.1, 158.6, 155.5, 152.2, 128.7, 128.7, 128.6, 126.5, 126.5, 126.4, 126.4, 126.4, 126.3, 113.0, 112.5, 101.5, 101.4, 101.2, 101.2, 101.2, 101.0, 100.9, 95.5, 88.2, 77.5, 77.2, 76.8, 56.0, 55.9. ^{19}F NMR (376 MHz, $CDCl_3$) δ ppm: -103.83, -103.86, -103.88, -105.97, -105.99. ESI-MS (*m/z*): [M + H]+ calculated at 363.08, found 363.18.

(*E*)-1-(4,6-Dimethoxybenzofuran-2-yl)-3-phenylprop-2-en-1-one (4n): Yield: 87%; m.f.: $C_{19}H_{16}O_4$; light-yellow colour; ^{1}H NMR (400 MHz, $CDCl_3$) δ ppm: 7.92 (d, *J* = 15.5 Hz, 1H), 7.70-7.68 (m, 3H), 7.51 (d, *J* = 15.5 Hz, 1H), 7.44 (m, 3H), 6.71 (s, 1H), 6.34 (s, 1H), 3.94 (s, 3H), 3.89 (s, 3H). ^{13}C NMR (101 MHz, $CDCl_3$) δ ppm: 178.4, 162.8, 158.2, 155.3, 152.2, 143.6, 134.8, 130.6, 129.0, 128.6, 121.4, 112.4, 95.3, 88.2, 56.0, 55.8. ESI-MS (*m/z*): $[M + H]^+$ calculated at 309.11, found 309.23.

(*E*)-1-(4,6-Dimethoxybenzofuran-2-yl)-3-(2,3,4-trimethoxyphenyl)prop-2-en-1-one (4o): Yield: 63%; m.f.: $C_{22}H_{22}O_7$; yellow colour; ^{1}H NMR (400 MHz, $CDCl_3$) δ ppm: 8.10 (d, *J* = 15.8 Hz, 1H), 7.68 (s, 1H), 7.54 (d, *J* = 15.8 Hz, 1H), 7.43 (d, *J* = 8.8 Hz, 1H), 6.75 (d, *J* = 8.8 Hz, 1H), 6.72 (s, 1H), 6.35 (d, *J* = 1.8 Hz, 1H), 4.00 (s, 3H), 3.95 (s, 3H), 3.94 (s, 3H), 3.92 (s, 3H), 3.90 (s, 3H,); ^{13}C NMR (101 MHz, $CDCl_3$) δ ppm: 178.9, 162.5, 158.1, 155.9, 155.2, 154.0, 152.6, 142.5, 139.0, 124.1, 122.0, 120.7, 112.4, 111.6, 107.6, 95.2, 88.1, 61.5, 61.0, 56.1, 55.9, 55.7. ESI-MS (*m/z*): $[M + H]^+$ calculated at 399.14, found 399.25.

***In vitro* anticancer activity:** The *in vitro* anticancer activity was assessed to determine the cell viability and cytotoxic effects of the synthesized compounds **4a-o** in A549) and MCF-7 cell lines using the 3-[4,5-dimethylthiazol-2-yl]-2,5-diphenyl tetrazolium bromide salt (MTT) assay, depending on the conversion of yellow tetrazolium salt to insoluble purple formazan crystals by mitochondrial enzymes in living cells [35]. The cell lines were cultivated in Dulbecco's modified Eagle's medium (DMEM) supplemented with 10% fetal bovine serum and 1% penicillin-streptomycin, providing a constant incubator temperature (37 ºC, 5% CO) to maintain the cell culture environment. The cells were cultivated in 96-well plates at a density of 10,000 cells/well for 24 h to allow cell attachment to the surface. The cells were then treated with different sample concentrations. Stock solutions of samples were prepared in DMSO and further diluted to obtain various concentrations (1000 µmol L^{-1}, 500 µmol L^{-1}, 250 µmol L^{-1}, 100 µmol L^{-1}, 50 µmol L^{-1}, 10 µµmol L^{-1} and 1.0 µmol L^{-1}) in an incomplete cell culture medium (without FBS). The untreated cells were used as a negative control and millepachine and paclitaxel were used as positive controls. MTT solution (20 µL) at a concentration of 5 mg/mL in phosphate-buffered saline was added to each well and the plates were incubated at 37 ºC in a CO incubator for 2 h. Finally, the compounds were centrifuged at 3000 rpm for 10 min and DMSO (100 µL) was added to stop the reaction and absorbance was measured at a wavelength of 540 nm using an ELISA microplate reader. The experiment was repeated in triplicate for each concentration and IC_{50} values and cell viability were analyzed using Microsoft Excel and GraphPad Prism 10.

Statistical analysis: All experiments were conducted in triplicate and the data presented as mean ± SEM. Analysis was assessed using one-way analysis of variance (ANOVA) followed by a post hoc Tukey's multiple comparison test below *p*-value 0.05 was considered statistically significant and two-way ANOVA revealed significant differences in IC_{50} values across cell lines ($p < 0.0001$) with post-hoc analysis. IC_{50} values were calculated for each compound determined using % cell viability values by GraphPad Prism10 software and Microsoft Excel.

Molecular docking: The synthesized chalcone compounds were screened for docking interactions to evaluate their binding to the tubulin colchicine site. The crystal structure of tubulin retrieved from the RCSB PDB database (PDB ID: 5JVD) [16,36,37] and tubulin structure was identified for missing residues, removing water molecules and cocrystal inhibitors, as well as extra chains removed, except the colchicine-binding pocket of tubulin chains A and B, which was saved in the PDB file using BIOVIA Discovery Studio 2024 [38] and PyMOL (version 3.0) [39].

Furthermore, the docking methodology was verified by redocking the extracted cocrystal chalcone TUB092 inhibitor (6NL) from the colchicine-binding pocket of tubulin using AutoDock4 Tools (ADL 1.5.7) [40,41], respectively. The 3D structure of the desired compound was generated by energy minimization and then saved in a Mol2 format file using ChemDraw [42] and Marvin (5.8.1) [43].

Tubulin protein was prepared for docking studies by incorporating Kollman's charges and adding polar hydrogens and torsions. The flexible docking simulations were assessed against millepachine by setting a grid box size of 60 × 60 × 60 points in the x, y and z directions with a center of 15.98, 68.251 42.958 and a grid spacing of 0.375 Å around the colchicine binding pocket of tubulin. One hundred runs were generated by applying Lamarckian genetic algorithm searches, employing default parameters of a population size of 150 individuals, a maximum of 2.5×10^7 energy assessments and a maximum of 2.7×10^4 generations. A gene mutation rate of 0.02 and a crossover rate 0.8 were selected. Docking data were assessed by obtaining docking log(dlg) output files and identifying the lowest energy protein-ligand interactions from the 10 docking poses

using the AutoDock4 suite and 2D and 3D interactions were visualized using Discovery Studio 2024 and PyMOL software.

***In silico* ADMET predictions:** In the preliminary stages of drug design, it is essential to optimize the pharmacodynamics and pharmacokinetics systematically, especially in terms of the administration, absorption, metabolism, excretion and toxicity (ADMET) properties of potential drug candidates. We used computational studies to predict the physico-chemical and pharmacokinetic properties of dimethoxy benzofuran-chalcones against millepachine using SwissADME Software Tools [44] and pkCSM [45] platform, considering parameters such as drug-likeness using Lipinski's rule of five [46], water solubility (logS), lipophilicity (logP), topological surface area (TSA), human intestinal absorption (HIA), human hERG potassium channels (related to cardiac toxicity), liver toxicity and inhibition of cytochrome P450 enzymes (CYP2D6 and CYP3A4).

RESULTS AND DISCUSSION

The Claisen-Schmidt condensation approach was used to synthesize novel chalcone derivatives (**4a-o, Scheme-II**) based on a molecular docking study. Initially, benzofuran **3**, key intermediate was obtained by the substitution and condensation of 2-hydroxy-4,6-dimethoxybenzaldehyde with chloroacetone in acetone and potassium carbonate, followed by reflux for 8 h. Finally, a series of chalcones **4a-o** were synthesized in 20-96% yield by Claisen-Schmidt condensation, mixing the solubilized benzofuran **3** mixtures in methanol at 40 ºC and the aldehyde with $Ba(OH)_2$ was stirred for 6 h until completion.

The synthesized compounds were analyzed for the ^{1}H NMR and ^{13}C NMR and mass (ESI-MS) spectrometry, the spectral data found correlates with predicted values and existing literature, validating the structural integrity and configuration of the synthesized compounds. The ^{1}H NMR spectra revealed a coupling constant > J = 15.0 Hz for both a and b-hydrogens, indicating an *E*-configuration of the chalcone structures. These outcomes provide a solid foundation for further biological studies.

Biological study

***In vitro* anticancer activity:** The cytotoxic efficacy of the synthesized dimethoxy benzofuran-chalcone compounds **4a-o** was assessed by the MTT assay in A549 and MCF-7 cell lines (Table-1 and Fig. 2). The IC_{50} values, signifying the concentration essential to inhibit 50% of cell viability, were measured using non-linear regression analysis of dose-response curves, which revealed a significant difference ($p < 0.001$) against the positive control, millepachine and paclitaxel, which are known tubulin-binding agents. Compounds **4m, 4f, 4n** and **4e** showed higher potency than the remaining compounds in the A549 cell line (Table-1, Fig. 2), while compounds **4i, 4h** and **4l** showed the best potency compared to other compounds in the MCF-7 cell line (Table-1, Fig. 2). In addition, One-Way ANOVA, followed by Tukey's multiple comparison test, revealed that there were no statistically significant differences in IC_{50} values across the compounds **4a-o** ($p > 0.05$) to the control. Notably, compound **4f** showed the highest potency in the lung cancer cell line A549 (IC_{50} = 23.9 µM), compared to a significantly lower effect in the breast cancer cell line MCF-7 (IC_{50} = 241 µM) (Table-1, Fig. 2). Similarly, compound **4m** showed moderate cytotoxicity in A549 cells (IC_{50} = 35.44 µM) and had reduced efficacy in MCF-7 cells (IC_{50} = 179.9 µM) (Table-1, Fig. 2). Conversely, compound **4l** demonstrated an IC_{50} value of 93.96 µM against MCF-7 cells, while indicating a decrease in A549 cell (IC_{50} =110 µM) as shown in Fig. 2. Moreover, two-way ANOVA revealed significant differences in IC_{50} values across cell lines ($p < 0.0001$) with post-hoc test analysis, which highlights the selective efficacy of the compounds towards A549 cells (Fig. 2). These results collectively suggest that the structural modification that enhances hydrophobic interactions and hydrogen bonding can further improve the anticancer activity of dimethoxy benzofuran-chalcone derivatives.

TABLE-1
MOLECULAR DOCKING AND *in vitro* ANTICANCER ACTIVITY OF SYNTHESIZED CHALCONE COMPOUNDS.
MOLECULAR DOCKING AND *in vitro* ANTICANCER ACTIVITY OF SYNTHESIZED CHALCONE COMPOUNDS

Compound	Binding energy (kcal/mol)	IC_{50} (µM ± SEM)	
		MCF-7	A549
4a	-9.26	409.8 ± 0.069	122.4 ± 0.221
4b	-9.33	574.2 ± 0.122	292.0 ± 0.150
4c	-9.23	444.9 ± 0.092	981.7 ± 0.086
4d	-9.69	226.5 ± 0.104	98.07 ± 0.129
4e	-9.17	289.6 ± 0.089	43.4 ± 0.246
4f	-9.94	241.0 ± 0.084	23.9 ± 0.203
4g	-9.66	404.6 ± 0.090	200.1 ± 0.181
4h	-9.92	99.97 ± 0.138	500 ± 0.287
4i	-9.63	99.51 ± 0.064	400.8 ± 0.132
4j	-9.30	146.7 ± 0.105	119.6 ± 0.097
4k	-9.24	216.9 ± 0.085	128.5 ± 0.124
4l	-9.21	93.96 ± 0.133	110 ± 0.135
4m	-9.19	179.9 ± 0.054	35.44 ± 0.135
4n	-9.00	182.1 ± 0.078	45.57 ± 0.201
4o	-9.89	545.8 ± 0.123	211.9 ± 0.216
Millepachine	-9.19	0.008 ± 0.002	0.220 ± 0.203
Paclitaxel	–	0.194 ± 0.130	0.0951 ± 0.206

Molecular docking: The redocking approach validated the docking methodology by binding the cocrystal 6NL inhibitor (chalcone TUB091) to the exact colchicine-binding site shown in the experimental structure of tubulin (PDB code 5JVD), as illustrated in Fig. 3, which confirms the accuracy and reliability of the docking protocol for evaluating the binding interactions of synthesized chalcones.

Molecular docking findings identified that synthesized chalcone derivatives **4a-o** were found interacting with the essential amino acids of colchicine-binding site of α,β-tubulin and obtained diverse binding affinities (B.E. = -9.0 kcal/mol to -9.92 kcal/mol) that were comparable and superior to millepachine (Table-1). These results suggest that chalcones adopt orientations similar to millepachine inside the colchicine-binding site, as shown in Fig. 4.

Chalcone compounds **4e**, **4f**, **4h**, **4i**, **4m**, **4l** and **4n** exhibited substantial hydrogen bonding, π-π stacking and hydrophobic contacts within the binding region, interacting with residues Met-259, Leu-255, Ala-250 Asn-350, Asn-258, Val-315, Cys-

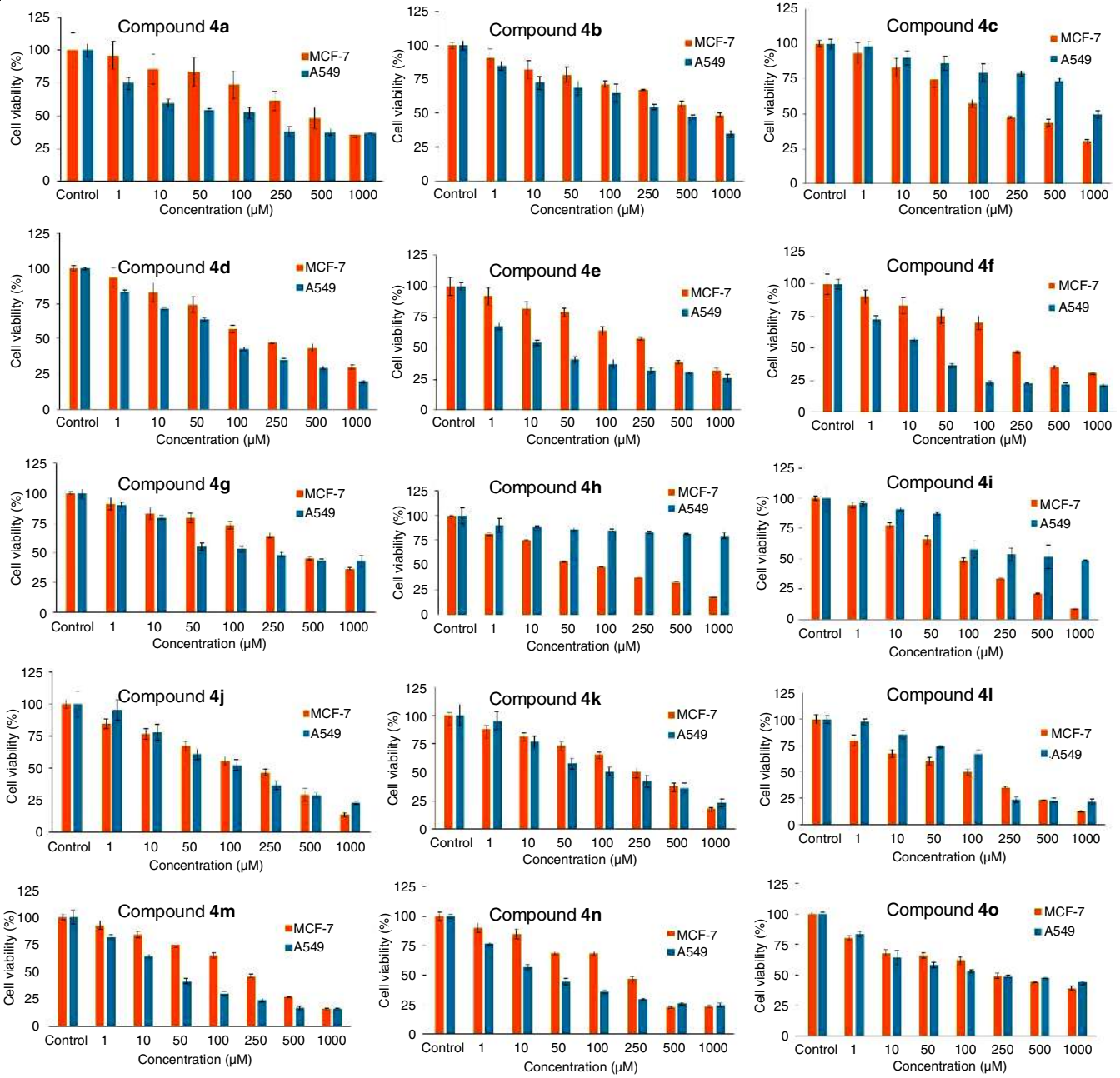

Fig. 2. The *in vitro* cell viability (%) assay of synthesized chalcone derivatives in A549 and MCF-7 cell lines

241 and Thr-179 of α,β-tubulin (Fig. 4). On the other hand, compounds **4m, 4l** and **4e** demonstrated enhanced stability of halogen bonding interactions with residue Asp-251, primarily through fluorine substitution on the benzene ring of chalcone (Fig. 4). Among all compounds, **4f** reported most favourable docking score (B.E. = -9.94 kcal/mol) with key residues Met-259 (pi-sulfur interaction), Asn-258 (H-bonding with the chalcone carbonyl group) and Leu-255 (hydrophobic contacts) binding pocket followed by compound **4h** (B.E. = -9.92 kcal/mol) as illustrated in Fig. 4.

***In silico* ADMET predictions:** *In silico* ADMET evaluation demonstrated that the synthesized compounds **4f**, **4h**, **4i**, **4l**, **4m**, **4n** had favourable physico-chemical and pharmacokinetics (ADMET) with acceptable drug-like characteristics, as tabulated in Table-2, including high oral bioavailability (HIA >99%), topological polar surface area (TPSA < 140A$^{2)}$), moderate lipophilicity (LogP value 1-5) and moderate Caco-2 permeability (log Papp range -4.63 to -4.73) against millepachine. Additionally, the plasma protein binding (PPB) showed fluctuation between compound **4i** (61.53%) and **4n** (78.45%), whereas **4i** and **4m** reported clearance rates ranging from 2.86 mL/min/kg to 6.85 mL/min/kg, which suggest moderate elimination capacity. Toxicity predictions indicated that all compounds were non-toxic to AMES mutagenicity and hERG inhibition, although compound **4o** displayed a slightly elevated risk of liver toxicity and carcinogenicity (Table-2). Among all the compounds, **4f** was found to be superior to millepachine in terms of Caco-2 permeability, lipophilicity and topological polar surface

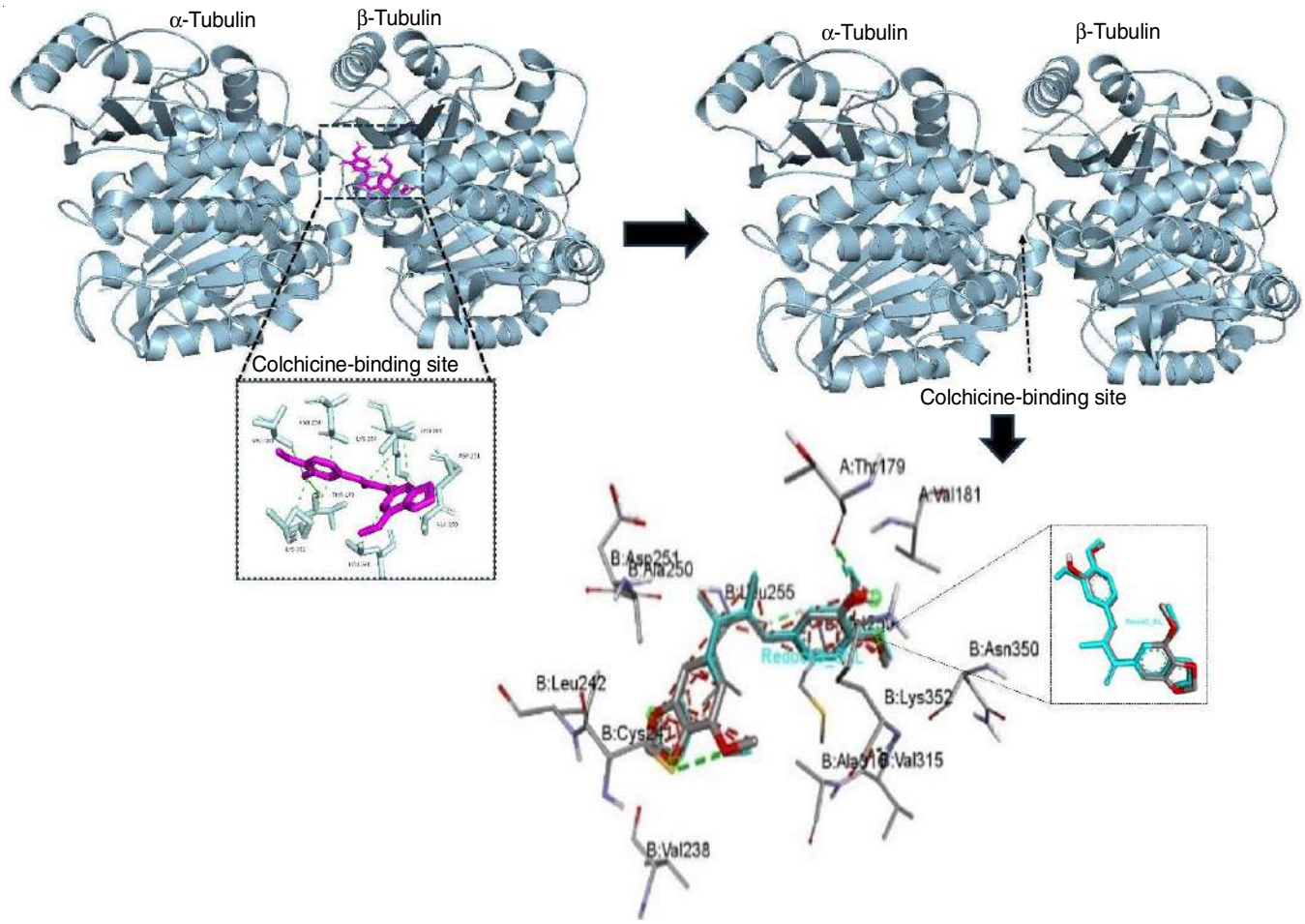

Fig. 3. The active site of the three-dimensional (3D) structure of α,β-tubulin protein (PDB ID: 5JVD) bound with a cocrystal 6NL inhibitor (chalcone, TUB091) and cleaned α,β-tubulin heterodimer. The redocked 3D structure of 6NL conformation superimposed with experimental structure of tubulin

TABLE-2
PHYSICO-CHEMICAL AND PHARMACOKINETIC PROPERTIES PREDICTION OF DIMETHOXY BENZOFURAN-CHALCONES AND A REFERENCE MILLEPACHINE USING pkCSM PLATFORM

Property	**4f**	**4h**	**4i**	**4l**	**4m**	**4n**	Millepachine
Molecular weight (g/mol)	338.35	368.38	368.38	362.3	362.3	308.33	320.38
Rotatable bonds (< 10)	6	7	7	5	5	5	4
H-bond acceptors (< 10)	5	6	6	7	7	4	3
H-bond donors (< 5)	0	0	0	0	0	0	0
Log(S)	-5.27	-5.43	-5.43	-5.32	-5.42	-5.42	-5.05
Log Po/w (1-3)	3.73	3.71	3.7	4.65	4.65	3.74	4.16
Topological polar surface area (< 140 Å^2)	57.9	67.13	67.13	48.67	48.67	48.67	35.53
Lipinski, violations	0	0	0	0	0	0	0
BBB permeability (%)	Yes	Yes	Yes	Yes	Yes	Yes	Yes
Caco-2 permeability	-4.7	-4.67	-4.65	-4.73	-4.53	-4.65	-4.82
Plasma protein binding (%)	67.22	62.59	61.53	78.22	78.45	74.01	61.2
Human oral bioavailability	Yes	Yes	Yes	Yes	Yes	Yes	Yes
Human intestinal absorption (%)	99.5	99.1	99.1	99.8	99.6	99.7	99.8
P-pg inhibitor	Yes	Yes	Yes	Yes	Yes	Yes	Yes
CYP2D6 inhibitor	No	No	No	No	No	No	No
CYP3A4 inhibitor	Yes	Yes	Yes	Yes	Yes	Yea	Yes
Clearance (mL/min/kg)	4.6	2.94	2.86	6.85	5.96	5.57	4.82
AMES toxicity	Safe	Safe	Safe	Safe	Safe	Safe	Safe
Carcinogenesis	Safe	Safe	Safe	Safe	Safe	LT	Safe
Liver toxicity (DILI)	LT	Safe	Safe	LT	LT	LT	Safe
hERG toxicity	Safe	Safe	Safe	Safe	Safe	Safe	Safe

LT = low toxicity

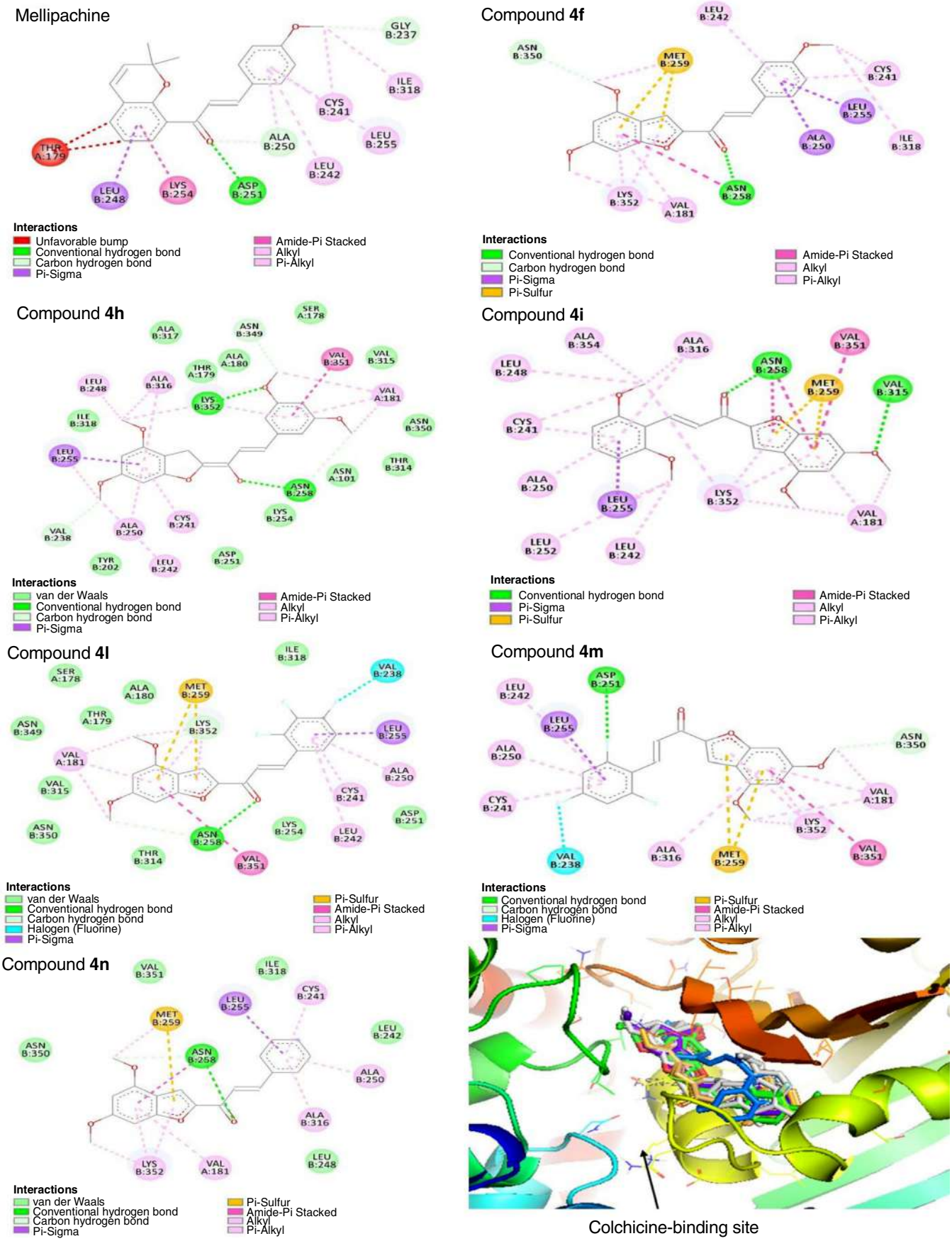

Fig. 4. The 2D structure interactions of dimethoxy benzofuran-chalcone compounds (**4f**, **4h**, **4i**, **4l**, **4m**, **4n**) and millepachine (reference). The 3D structures of chalcone compounds superimposed with reference in the colchicine-binding site of α,β-tubulin

area, indicating enhanced absorption and permeability and a low plasma protein binding (67.22%), which suggest improved free drug availability as shown in Table-2.

Structure-activity relationship (SAR): The structure-activity relationship (SAR) of dimethoxy benzofuran-chalcones **4a-o** was identified to determine the key features for activity and how to improve the compounds' potency, specificity and other desirable properties [47] (Fig. 5). The synthesized novel chalcone compounds showed anticancer effects through interactions with critical residues Met-259, Leu-255, Ala-250, Asn-350 and Thr-314 in the colchicine-binding region of α,β-tubulin (Fig. 4). The planar aromatic structure of the benzofuran core of chalcone promotes strong π-sulfur interactions with the hydrophobic residue Met-259 as well as hydrogen bonding with the polar residues Asn-350 and Thr-314 binding site of β-tubulin. Furthermore, the incorporation of electron-donating groups (EDGs) such as -OCH_3 and the substitution of electron-withdrawing groups (EWGs) at the C4 and C6 positions of the benzofuran core could enhance compound stabilization within the binding domain, as shown in Fig. 4. Similarly, replacing the halogen groups on the phenyl ring of chalcone (*e.g.* -F > -Cl > -Br > -CF_3) improved halogen bonding, whereas the introduction of a methoxy group (-OCH_3) at C-4 enhanced H-bonding with α,β-tubulin binding pocket. Substitution of trifluoromethyl (-CF_3) at the C-4 position of the phenyl ring resulted in diminished efficacy. The linker region provided flexibility and alignment inside the binding region, with a carbonyl moiety forming H-bonds with the Asn-350 and Lys-352 residues and the saturated α and β bonds maintained a planar configuration within the colchicine-binding domain (Fig. 4). The SAR findings provide a foundation for future structural optimization and mechanistic studies of dimethoxy benzofuran-chalcones.

Conclusion

In this study, a series of novel dimethoxy benzofuran-chalcone derivatives (**4a-o**) were designed, synthesized and assessed to target the colchicine-binding site of tubulin by performing *in silico* docking studies and *in vitro* anticancer activity using the MTT assay in A549 and MCF-7 cell lines. The synthesized compounds **4f**, **4h**, **4i**, **4l**, **4m** and **4n** showed promising anticancer activity and were not significantly different in the case of IC_{50} values (One-Way ANOVA, $p > 0.05$) to the control. However, chalcone derivatives showed notable selectivity and good potency towards A549 cell line (two-way ANOVA, $p < 0.0001$), such as compounds **4f** (IC_{50} = 23.90 μM) and **4m** (IC_{50} = 35.44 μM). Moreover, in the MCF-7 cell line, compounds **4f** and **4m** showed reduced potency, with IC_{50} values of 241 μM and 179.9 μM, respectively. Docking studies have suggested favourable pharmacokinetics and robust binding interactions within the colchicine-binding domain of α,β-tubulin. Additionally, compound **4g** displayed a strong binding affinity -9.94 kcal/mol with crucial residues at the tubulin colchicine site. Future research will explore the *in vitro* anticancer efficacy across other cancer cell lines and identify the molecular mechanisms.

ACKNOWLEDGEMENTS

One of the authors, Kailash Rani acknowledge Dr. Anju Goyal, University School of Pharmaceutical Sciences, Rayat Bahra University, Mohali, Punjab, India for contributing to the scientific discussion.

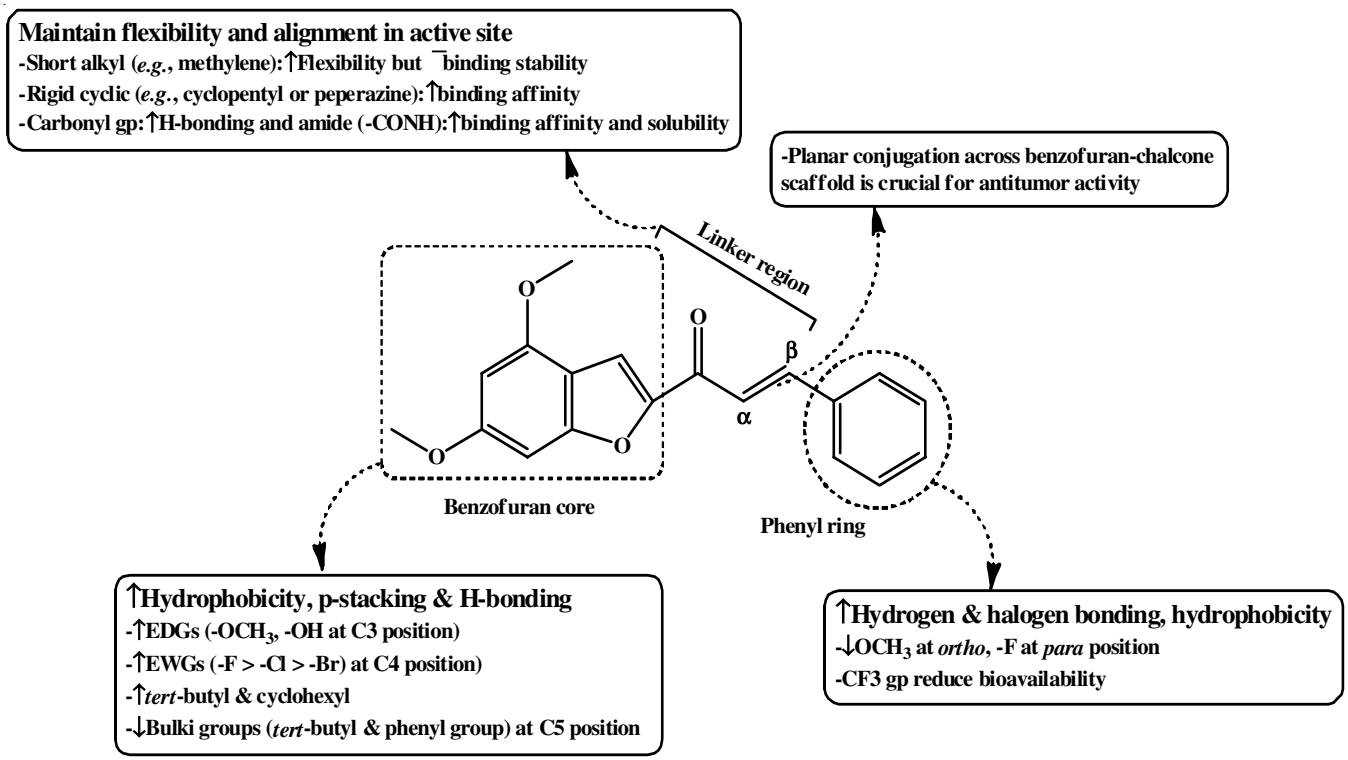

Fig. 5. Structure-activity relationship of the dimethoxy benzofuran-chalcone

CONFLICT OF INTEREST

The authors declare that there is no conflict of interests regarding the publication of this article.

REFERENCES

1. H. Sung, J. Ferlay, R.L. Siegel, M. Laversanne, I. Soerjomataram, A. Jemal and F. Bray, *CA Cancer J. Clin.*, **71**, 209 (2021); https://doi.org/10.3322/caac.21660
2. R.L. Siegel, A.N. Giaquinto and A. Jemal, *CA Cancer J. Clin.*, **74**, 12 (2024); https://doi.org/10.3322/caac.21820
3. F. Bray, M. Laversanne, H. Sung, J. Ferlay, R.L. Siegel, I. Soerjomataram and A. Jemal, *CA Cancer J. Clin.*, **74**, 229 (2024); https://doi.org/10.3322/caac.21834
4. D. Hanahan and R.A. Weinberg, *Cell*, **144**, 646 (2011); https://doi.org/10.1016/j.cell.2011.02.013
5. F. Bray, M. Laversanne, E. Weiderpass and I. Soerjomataram, *Cancer*, **127**, 3029 (2021); https://doi.org/10.1002/cncr.33587
6. J. Zhou and P. Giannakakou, *Curr. Med. Chem. Anticancer Agents*, **5**, 65 (2005); https://doi.org/10.2174/1568011053352569
7. M.A. Jordan and L. Wilson, *Nat. Rev. Cancer*, **4**, 253 (2004); https://doi.org/10.1038/nrc1317
8. C. Dumontet and M.A. Jordan, *Nat. Rev. Drug Discov.*, **9**, 790 (2010); https://doi.org/10.1038/nrd3253
9. M.A. Jordan and K. Kamath, *Curr. Cancer Drug Targets*, **7**, 730 (2007); https://doi.org/10.2174/156800907783220417
10. J. Sebastian and K. Rathinasamy, *Curr. Drug Targets*, **24**, 889 (2023); https://doi.org/10.2174/1389450124666230731094837
11. A.E. Prota, K. Bargsten, D. Zurwerra, J.J. Field, J.F. Díaz, K.-H. Altmann and M.O. Steinmetz, *Science*, **339**, 587 (2013); https://doi.org/10.1126/science.1230582
12. E. Pasquier and M. Kavallaris, *IUBMB Life*, **60**, 165 (2008); https://doi.org/10.1002/iub.25
13. B.A. Weaver, *Mol. Biol. Cell*, **25**, 2677 (2014); https://doi.org/10.1091/mbc.e14-04-0916
14. M. Kavallaris, *Nat. Rev. Cancer*, **10**, 194 (2010); https://doi.org/10.1038/nrc2803
15. R. Wang, S. Lin, Y. Wang, W. Qian and L. Zhou, *PLoS One*, **12**, e0175985 (2017); https://doi.org/10.1371/journal.pone.0175985
16. M.-D. Canela, S. Noppen, O. Bueno, A.E. Prota, K. Bargsten, G. Sáez-Calvo, M.-L. Jimeno, M. Benkheil, D. Ribatti, S. Velázquez, M.-J. Camarasa, J. Fernando-Díaz, M.O. Steinmetz, E.-M. Priego, M.-J. Pérez-Pérez and S. Liekens, *Oncotarget*, **8**, 14325 (2017); https://doi.org/10.18632/oncotarget.9527
17. S. Rampogu, P. Badvel, B.H. Jo, Y. Kim, S.-W. Kim and K.W. Lee, *Biochem. Biophys. Res. Commun.*, **681**, 249 (2023); https://doi.org/10.1016/j.bbrc.2023.09.044
18. W. Wu, H. Ye, L. Wan, X. Han, G. Wang, J. Hu, M. Tang, X. Duan, Y. Fan, S. He, L. Huang, H. Pei, X. Wang, X. Li, C. Xie, R. Zhang, Z. Yuan, Y. Mao, Y. Wei and L. Chen, *Carcinogenesis*, **34**, 1636 (2013); https://doi.org/10.1093/carcin/bgt087
19. V. Peyrot, D. Leynadier, M. Sarrazin, C. Briand, A. Rodriquez, J.M. Nieto and J.M. Andreu, *J. Biol. Chem*., **264**, 21296 (1989); https://doi.org/10.1016/S0021-9258(19)30078-X
20. T. Vishnu, M. Veerabhadraiah, V. Krishna Chaitanya, M. Nagamani, M. Raghavender and P. Jalapathi, *Mol. Divers.*, **27**, 2695 (2023); https://doi.org/10.1007/s11030-022-10575-6
21. Y. Liu, C. Zhang, X. Zhang, C. Wan and Z. Mao, *Chem. Biodivers.*, e202401991 (2024); https://doi.org/10.1002/cbdv.202401991
22. W.M. Eldehna, R. Salem, Z.M. Elsayed, T. Al-Warhi, H.R. Knany, R.R. Ayyad, T.B. Traiki, M.-H. Abdulla, R. Ahmad, H.A. Abdel-Aziz and R. El-Haggar show less, *J. Enzyme Inhib. Med. Chem.*, **36**, 1424 (2021); https://doi.org/10.1080/14756366.2021.1944127
23. M.J. Mphahlele, M.M. Maluleka, N. Parbhoo and S.T. Malindisa, *Int. J. Mol. Sci.*, **19**, 2552 (2018); https://doi.org/10.3390/ijms19092552
24. C. Zhang, Y. Liu, X. Zhang, C. Wan and Z. Mao, *RSC Med. Chem.*, (2024); https://doi.org/10.1039/D4MD00621F
25. S. Cinar-Asa, D. Coskun, O. Akgun, H. Akgun, M. Fatih Coskun and F. Ari, *ChemistrySelect*, **8**, e202204402 (2023); https://doi.org/10.1002/slct.202204402
26. A.A. Abbas and K.M. Dawood, *RSC Adv.*, **13**, 11096 (2023); https://doi.org/10.1039/D3RA01383A
27. V. Peyrot, D. Leynadier, M. Sarrazin, C. Briand, M. Menendez, J. Laynez and J.M. Andreu, *Biochemistry*, **31**, 11125 (1992); https://doi.org/10.1021/bi00160a024
28. B. Komuraiah, Y. Ren, M. Xue, B. Cheng, J. Liu, Y. Liu and J. Chen, *Chem. Biol. Drug Des.*, **97**, 1109 (2021); https://doi.org/10.1111/cbdd.13832
29. M. Jumaah, T.D. Wahyuningsih and M. Khairuddean, *Indo. J. Chem.*, **22**, 1246 (2022); https://doi.org/10.22146/ijc.72790
30. K. Bowden, C. Duah and R.J. Ranson, *J. Chem. Soc., Perkin Trans. 2*, 109 (1991); https://doi.org/10.1039/p29910000109
31. T. Moriya, A. Kawamata, Y. Takahashi, Y. Iwabuchi and N. Kanoh, *Chem. Commun.*, **49**, 11500 (2013); https://doi.org/10.1039/C3CC47264G
32. K.M. Dawood, *Expert Opin. Ther. Pat.*, **23**, 1133 (2013); https://doi.org/10.1517/13543776.2013.801455
33. I. Alioglu, S. Cinar-Asa, D. Coskun and F. Ari, *Iran. J. Sci.*, **47**, 1057 (2023); https://doi.org/10.1007/s40995-023-01494-8
34. D. Coskun, M. Erkisa, E. Ulukaya, M.F. Coskun and F. Ari, *Eur. J. Med. Chem.*, **136**, 212 (2017); https://doi.org/10.1016/j.ejmech.2017.05.017
35. J. van Meerloo, G.J.L. Kaspers and J. Cloos, *Methods Mol. Biol.*, **731**, 237 (2011); https://doi.org/10.1007/978-1-61779-080-5_20
36. J. Yang, W. Yan, Y. Yu, Y. Wang, T. Yang, L. Xue, X. Yuan, C. Long, Z. Liu, X. Chen, M. Hu, L. Zheng, Q. Qiu, H. Pei, D. Li, F. Wang, P. Bai, J. Wen, H. Ye and L. Chen, *J. Biol. Chem.*, **293**, 9461 (2018); https://doi.org/10.1074/jbc.RA117.001658
37. X. Huang, M. Wang, C. Wang, W. Hu, Q. You, T. Ma, Q. Jia, C. Yu, Z. Liao and H. Wang, *Bioorg. Chem.*, **94**, 103486 (2020); https://doi.org/10.1016/j.bioorg.2019.103486
38. D. Systèmes, BIOVIA Discovery Studio Visualizer - Dassault Systèmes (2020); https://discover.3ds.com/discovery-studio-visualizer-download
39. Schrödinger, LLC, The PyMOL Molecular Graphics System, Version 1.8 (2015).
40. S. Forli, R. Huey, M.E. Pique, M.F. Sanner, D.S. Goodsell and A.J. Olson, *Nat. Protoc.*, **11**, 905 (2016); https://doi.org/10.1038/nprot.2016.051
41. G.M. Morris, R. Huey, W. Lindstrom, M.F. Sanner, R.K. Belew, D.S. Goodsell and A.J. Olson, *J. Comput. Chem.*, **30**, 2785 (2009); https://doi.org/10.1002/jcc.21256
42. Z. Li, H. Wan, Y. Shi and P. Ouyang, *J. Chem. Inf. Comput. Sci.*, **44**, 1886 (2004); https://doi.org/10.1021/ci049794h
43. Marvin Desktop Suite, Chemaxon Docs; https://docs.chemaxon.com/display/docs/marvin-desktop-suite.md
44. A. Daina, O. Michielin and V. Zoete, *Sci. Rep.*, **7**, 42717 (2017); https://doi.org/10.1038/srep42717
45. D. Pires, T. Blundell and D.B. Ascher, *J. Med. Chem.*, **58**, 4066 (2015); https://doi.org/10.1021/acs.jmedchem.5b00104
46. C.A. Lipinski, *J. Pharmacol. Toxicol. Methods*, **44**, 235 (2000); https://doi.org/10.1016/S1056-8719(00)00107-6
47. D.T. Chu and P.B. Fernandes, *Antimicrob. Agents Chemother.*, **33**, 131 (1989); https://doi.org/10.1128/AAC.33.2.131